Journal of Visualization, Vol. 12, No. 4 (2009) 339-346

Regular Paper

Splash Formation by a Spherical Body Plunging into Water

Kubota, Y.*[1] and Mochizuki, O.*[2]

*1 Graduate School of Engineering, Toyo University, 2100 Kujirai, Kawagoe, Saitama 350-8585, Japan.
E-mail: dn0800032@toyonet.toyo.ac.jp
*2 Faculty of Science and Engineering, Toyo University, 2100 Kujirai, Kawagoe, Saitama 350-8585, Japan.

Received 21 January 2009
Revised 24 May 2009

Abstract : Splashes caused by a spherical body plunging into water were investigated experimentally using a high speed CMOS camera. We categorized types of splash according to impact velocities of the sphere. Three types of splash were found: Type-I is a thin spire-type splash, Type-II is a mushroom-type splash with many droplets, and Type-III is a crown-type splash with many droplets. The reaction to the concave water surface attached to the sinking sphere is a cause of the Type-I splash. The film flow climbing up the sphere is a dominant cause of the Type-II splash. The velocity of the film flow, which is proportional to the impact velocity of the sphere, affects the fingers of the film flow, detaching of droplets, and maximum height of the Type-II splash. The Type-III crown-type splash is characterized by water jets with many droplets. A bulky air column in water is formed behind the sinking sphere, and longitudinal ridges and ripples on the surface of the air column were observed.

Keywords : Visualization, Water splash, Solid sphere, Film flow, High speed CMOS video camera.

1. Introduction

Splashes formed by a spherical body plunging into water were investigated experimentally. The objective of this study is to categorize splash patterns for different impact velocities of the sphere. Water splashes appear in the following cases: a liquid–liquid collision, droplets impinging on a solid surface, and a solid body impinging on a liquid surface. In an example practical application of the latter case, a wedge-shape body impacting water was studied to better understand seaplane landing by von Karman (1929). The relationship between gliding angle, landing speed, and downward velocity of the seaplane was analyzed. Sound from a body or droplet impacting water can produce problems in real applications, and the relationship between water splash and sound generation was reported by Duez et al. (2007). They observed splash patterns, but not the details of their formation. A splash is also formed by a droplet impacting a solid surface. The finger-like structures at the circumferential edge of water film flow spreading in the radial direction were reported by Yoon et al. (2007). Bejan et al. (2006) and Bussmann et al. (2000) numerically and experimentally investigated the deformation of a droplet impinging on a solid surface. The number of fingers of the spreading droplet after collision was described by Rayleigh–Taylor instability theory. The linear perturbation theory for interface instability of a radially expanding liquid sheet was studied by Kim et al.(2000) for droplet collisions with a solid surface. These studies are useful in understanding the finger-like structures of the film flow climbing up the sphere upon impacting water in our observations. To understand the mechanism of finger generation, we compared our results with previous studies of

spreading water film flow. For the liquid–liquid collision, three types of collision for two drops were reported by Testik et al. (2008). They showed that the manner of collision changed with the size and approaching direction of droplets. The milk crown from a milk droplet and solid body falling into milk was studied by Worthington (1882). They showed splash patterns, but did not discuss details on classification and generation mechanisms.

The water splash is similar to the above studies, but details of its formation are not well known. We categorized types of splash according to impact velocities of the sphere. Three types of splash were found: Type-I is a thin spire-type splash, Type-II is a mushroom-type splash with many droplets, and Type-III is a crown-type splash with many droplets. Characteristics for these splash types are discussed in this study.

2. Experimental Setup

Experiments of a spherical body impinging on water were performed. A 300 × 300 × 400 mm^3 tank was filled with water up to a height of 340 mm. Tap water was used in this experiment as the results are insensitive to the difference between tap and distilled water, as shown in Fig. 1. The sequence of splash-formation photos for tap and distilled water taken with the same timing coincide with each other. Thus, any contaminants in the tap water do not affect the results.

An acrylic sphere with diameter $D (= 2R) = 20$ mm and mass $M = 4.8 \times 10^{-3}$ kg was used in this experiment. The surface of sphere was hydro dynamically smooth, and the surface roughness of sphere has not changed during the experiment. The surface of the sphere was carefully cleaned for stains such as oil before each trial to maintain controlled surface conditions. The free-fall velocity of the sphere was varied by changing the initial height h, which is measured from the water surface to the bottom of the sphere. The initial height h was varied from $0.1D$ to $66D$, which results in the impact velocity V_i of the sphere at the water surface varying from 0.10 to 5.09 m/s. V_i was determined from the conservation of energy, and is given by $V_i = (2gh)^{0.5}$, because air drag is negligible for the range of heights in this study. A pipe held the sphere via suction at the initial height just before release. We release the sphere by turning off the electric valve to the suction pipe, and this enables the sphere to fall without rotation or horizontal displacement, producing reproducible results.

The sequence of splash formation was photographed from the side and top of the water tank using a high speed CMOS camera (Vision Research Inc., Phantom v7.1). The camera was set at

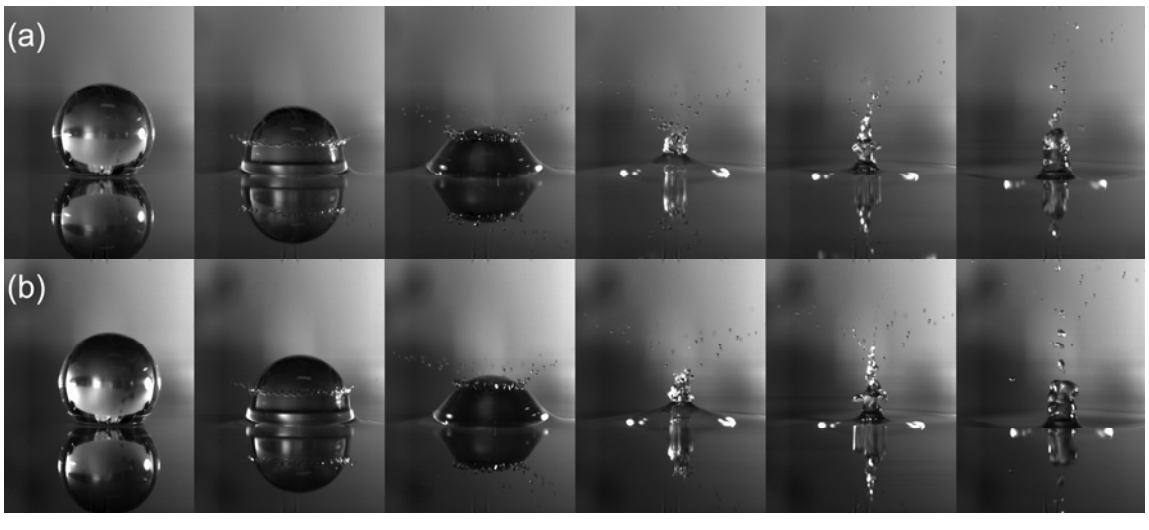

Fig.1. Comparison between sequences of water splash formation for (a) tap water and (b) distilled water in the case of V_i = 1.4 m/s. As the difference was negligible, effects of contaminants in the tap water were not important in our experiment.

4000 frames per second so that precision in timing between consecutive frames was 0.25 ms. A halogen lamp of 500 W was used for illuminating the splash.

3. Experimental Results and Discussions

Two important dimensionless parameters for splash formation are the Reynolds number Re and the Weber number We. The former is defined as $Re = V_i D/\nu$, where ν is the kinematic viscosity of water at 25°C, and the latter is given by $We = \rho V_i^2 D/\sigma$, where ρ is the density and σ is the surface tension of water at 25°C. The dimensionless time T is defined as $T = tV_i/D$, where t is the measured time. This is useful for comparing splashes formed at different V_i. Even if V_i is different, $T = 1$ indicates the same dimensionless time interval while the sphere moves a distance equal to the diameter D. $T = 0$ when the sphere touches the water surface.

3.1 Classification of Splash Formation

Various types of water splash for different V_i were observed. We categorized water splashes by similarity in the formation process, as shown in Fig. 2. The splash categorization is discussed in this section, and details on each type are discussed in the following sections. The splash formation is classified into three types: Type-I, -II, and -III. The horizontal axis in Fig. 2 shows the impact velocity V_i, and vertical axis shows the dimensionless time T_s when a splash is first observed. Circular marks in the figure show the beginning of splash formation for different V_i. The Type-I splash appears in the range of $0 < V_i < 0.9$ m/s. The splash is similar to a thin spire and its formation process is the same in this range. The details for the Type-I splash are presented in Section 3.2. The Type-II splash appears in the range of $0.9 \leqq V_i < 4.2$ m/s. The value of V_i at the border between Type-I and Type-II is 0.9 m/s $\pm$0.1 m/s. The splash shape is similar to a mushroom with small droplets, and a thin film flow along the sphere surface before splash formation is a peculiarity of Type-II. The details for the Type-II splash are presented in Section 3.3. The Type-III splash appears in the range of $4.2 \leqq V_i \leqq 5.1$ m/s. The value of V_i at the border between Type-II and Type-III is 4.2 m/s $\pm$0.1 m/s, and $V_i = 5.1$ m/s is the upper limit of our experiments. Characteristics of Type-III splashes are a crown shape with small droplets and a large air column following the sphere after water entry. The details for the Type-III splash are presented in Section 3.4.

$T_s = t_s V_i/D$ shows non-dimensional time of t_s. t_s is the beginning time when the spire-type, mushroom-type and crown-type splashes form for each case. The time at which splash formation begins, T_s, represented by a solid circular mark, is continuous, indicating that there is no apparent timing jump for splash formation even if the formation process is different for each type. T_s in Type-I increases with increasing V_i until V_i becomes 0.52 m/s, where T_s becomes maximum, and it decreases when $V_i > 0.52$ m/s. On the other hand, T_s in Type-II decreases with increasing V_i until $V_i = 2.8$ m/s, and plateaus in the range of $2.7 < V_i < 4.2$ m/s. T_s in Type-III linearly decreases with increasing V_i. The reason why T_s changes in such a manner is yet unclear. It is

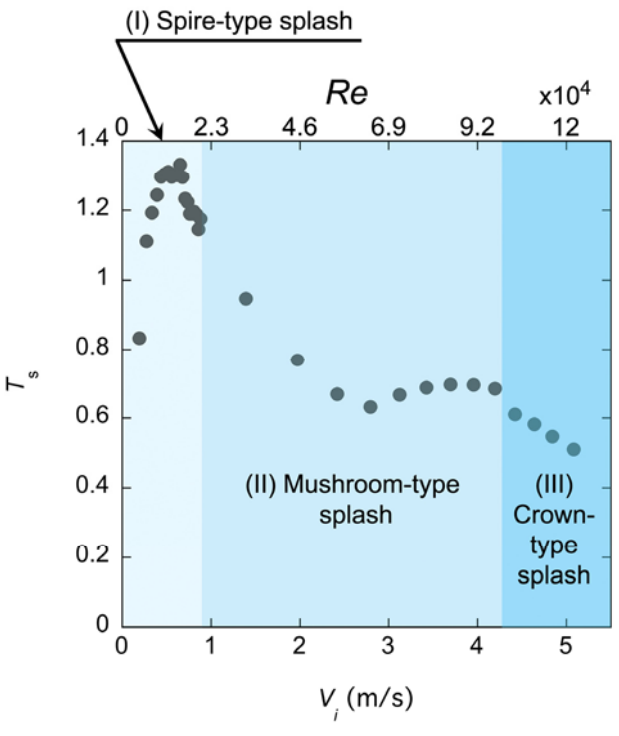

Fig.2. Timing of splash formation for different impact velocities of sphere and classification of types of splash.

encouraging that our categorization is similar to that given by Duez et al. (2007) who reported the effect of surface coating on splash type boundaries. Our findings for the splash formation start times may be the key in understanding the physics of splash formation.

3.2 Splash formation of Type-I

A typical splash in Type-I is shown in Fig. 3, where V_i = 0.20 m/s. The dimensionless parameters are $Re = 4.5 \times 10^3$ and $We = 1.1 \times 10^1$. To calculate these numbers, we used the diameter of the sphere as a characteristic length. The process of splash formation once the sphere enters water after touching the water surface is as follows: 1) a bump appears around the sphere as shown in T=0.22, 2) a concave water surface attaches behind the sphere as shown in T=0.67, 3) the concavity detaches as shown in T=0.89, and a thin spire splash develops.

The detachment occurs just before T = 0.89 in this case, as shown in Fig. 3. The spire-type splash is formed in reaction to the concavity. As observed in Fig. 3, small droplets part from the tip of the thin splash. The formation of these droplets arises due to the surface instability of the thin water column, and this is related to the Weber number for the splash We_s =2.2x10^2 based on its diameter and rising velocity. The critical Weber number We_c for droplet breakup is given by $We_c = 11.5 D_d^{-0.209}$, where D_d is the diameter of droplet, obtained by Yoshida (1997). We_c in our case was 4.9×10^1. As We_s of the spire-type splash exceeds We_c, droplets separate from the tip of this splash.

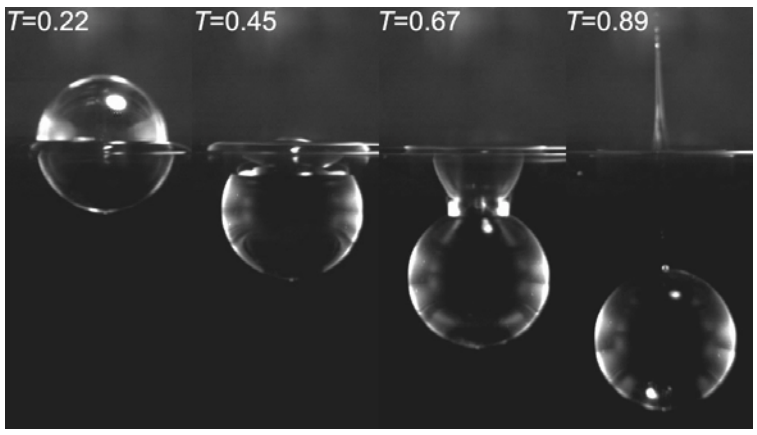

Fig.3. Spire-like Type-I splash at V_i=0.20 m/s.

Another interesting observation is a small bubble attaching at the rear stagnation point of the sphere, as observed in Fig. 3. This bubble is formed when the concavity detaches itself from the sphere. Vibration of the bubble can generate pure sound.

3.3 Splash formation of Type-II

Two typical sequences of Type-II splash formation are shown in Fig. 4, representing the decreasing and increasing trends in T_s ,as observed in Fig. 2 for Type-II. The photos in Fig. 4(a) are taken in the case of V_i = 1.4 m/s, $Re = 3.2 \times 10^4$, and $We = 5 \times 10^2$, and the ones in Fig. 4(b) represent the case of V_i = 3.1 m/s, $Re = 7.2 \times 10^4$, and $We = 2.7 \times 10^3$. The pictures taken at the same T for the two cases look similar except for details that will be discussed later, i.e., general changes in Type-II are categorized by T as follows: 1) film flow with a wavy top edge rises along the sphere at T = 0.12, just after impingement on the water surface, 2) the film flow rises and develops a wavy top edge (called fingers hereafter), and small droplets detach from finger summits at T = 0.25, 3) film flow fingers meet at the rear of the sphere at T = 0.72, and 4) a mushroom splash with droplets grows at T = 1.14, just after the sphere goes under water. The concavity following the sphere does not appear in Type-II. The film flow covers the sphere so that air does not entrain.

The detailed difference in phenomena at the same T in Figs. 4(a) and (b) are as follows. The film flow at T = 0.12 in Fig. 4(b) is higher than that in Fig. 4(a), indicating that the maximum velocity V_{fmax} at the top of the film flow ascent is faster in Fig. 4(b), i.e., V_{fmax} is faster when V_i is faster. Figure 5 shows V_{fmax} measured at T = 0.05 for different V_i in Type-II. V_{fmax} is proportional to 8.3 V_i, implying that the kinetic energy of the sphere at impact transfers to that of the film flow. Thus, the maximum rising velocity of the film flow is given by $V_{fmax} = V_i \sqrt{M/m_f}$. If the experiment is carried out with the difference mass of model, M, and the same impact velocity V_i, the maximum film velocity, V_{fmax}, might be changed. From this relationship, we can obtain the average mass of the film

flow, m_f, to be 7.0×10^{-5} kg and the average thickness of the film flow to be 2.2×10^{-3} m because the height of the film flow is 1.0×10^{-3} m at $T = 0.05$.

The initial separation of the film flow from the sphere appears to occur earlier with increasing V_i, as observed in Fig. 4, with $T = 0.12$. The initial separation angle is measured from the bottom of the sphere to the point where the film flow separates, as shown for Type-II in Fig. 6 for different V_i is about 80 degrees at $V_i = 1.4$ m/s and is about 20 degrees for $V_i = 4.2$ m/s. The initial separation angle becomes smaller with increasing V_i, i.e., the separation occurs earlier when V_i becomes large. This is a result of the competition between the centrifugal and adhesive forces acting on the film flow. The centrifugal force increases with increasing V_{fmax} according to $m_f V_{fmax}^2 / R$. Here, R is the radius of sphere. As $V_{fmax} = V_i \sqrt{M/m_f}$, as described above, the centrifugal force increases when V_i increases. If the centrifugal force exceeds the adhesive force, the top of the film flow separates from the surface. This suggests that there may be no droplet separation for a body shape without a means to generate centrifugal force, such as a body with no curvature. The wavy top edge of the film flow with droplets meet at the rear of the sphere at $T = 0.72$ in Fig. 4. The meeting time is earlier with increasing V_i.

The small droplets detach from the summits of the fingers. The number of droplets detached from tips of fingers increases with increasing V_i, as observed in the pictures at $T = 0.72$ and 1.14. This is because the number of fingers also increases when V_i is faster, as observed in the comparison photos at $T = 0.12$ and 0.25 for Type-II. The number of fingers is plotted against the Weber number in Fig. 7. We was based on V_i and the diameter of the film flow, which is equal to the diameter of the sphere in this experiment. The number of fingers, n, was counted when the top of the film flow reached half of the sphere. The circular marks show our experimental results, and solid line shows the analytical result obtained via Rayleigh–Taylor instability theory (Allen, 1975). The analytical finding was obtained in the case of a spreading droplet on a solid surface after impact, resulting in the relation $n = We^{1/2} \mathrm{Re}^{1/4} / \left(4\sqrt{3}\right)$. Our experimental result is in good agreement with the analytical one.

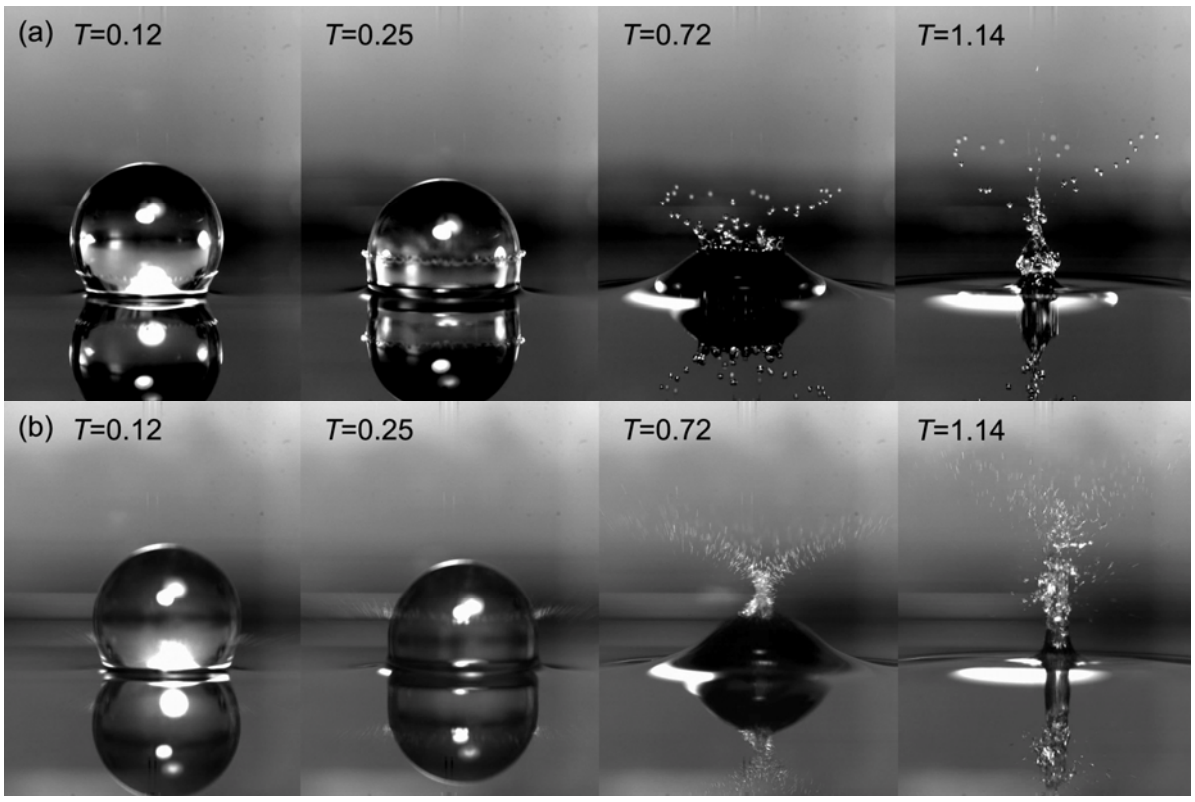

Fig.4. Sequence of Type-II splash formation. (a) $V_i = 1.4$ m/s, (b) $V_i = 3.1$ m/s.

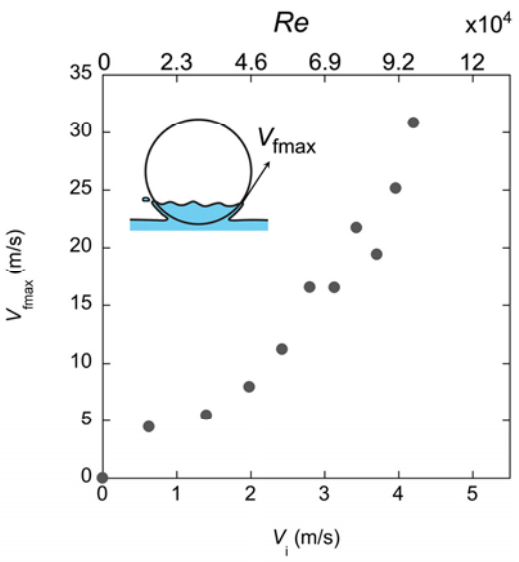

Fig.5. Velocity (V_{fmax}) of film-flow measured at T=0.05 for different V_i.

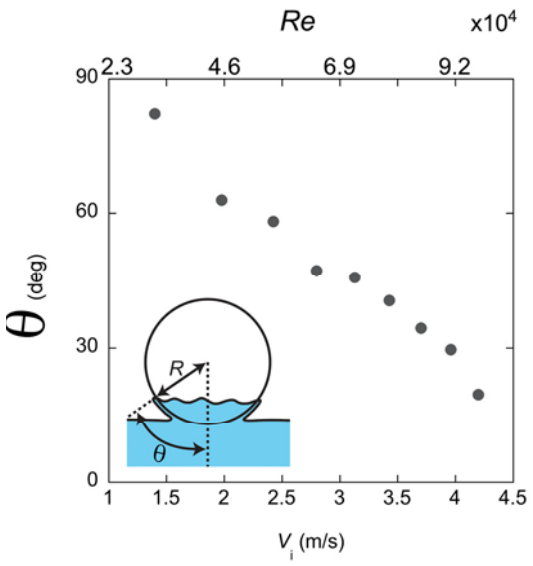

Fig.6. Separation angle of droplets for different V_i.

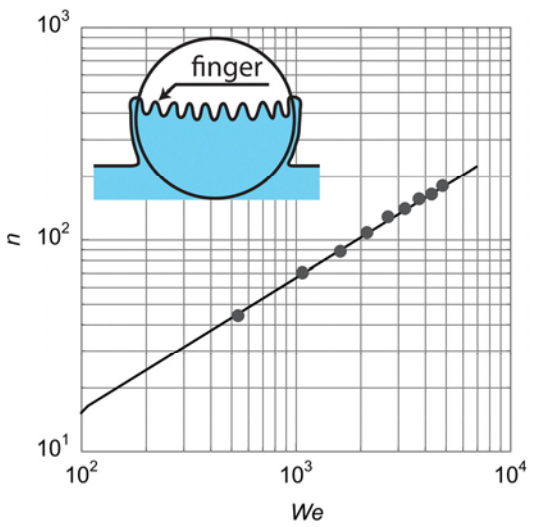

Fig.7. Number of fingers observed at l=62mm (circumference) vs. Weber number (We).
●: Measured,
—: $n = We^{1/2}\,\mathrm{Re}^{1/4}\Big/\left(4\sqrt{3}\right)$ Analytical result (Allen, 1975)

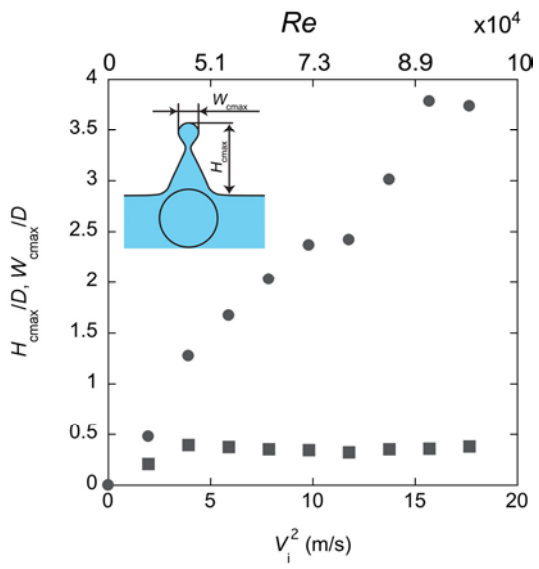

Fig.8. Dependence on energy for the dimensionless maximum height (H_{cmax}/D) and the dimensionless width (W_{cmax}/D) of water column. ●: H_{cmax}/D, ■: W_{cmax}/D

A mushroom splash with droplets grows at T = 1.14 just after the sphere goes under water, as observed in Fig. 4. The change in size of the mushroom splash is shown in Fig. 8 for different V_i^2. The dimensionless maximum height of the mushroom splash, H_{cmax}/D, is shown with circular marks, and the dimensionless width of the head of the mushroom splash, W_{cmax}/D, is shown with square marks in the figure. The height of the mushroom increased in proportion to V_i^2, as expected for a transfer of kinetic energy from the impacting sphere to the potential energy of the mushroom. On the other hand, the diameter of droplet is almost constant and equal to $0.34D$. In this case, $We = 7.0 \times 10^2$ for the head of mushroom exceeds $We_c = 3.3 \times 10^1$. Thus, the inertia of the head of the mushroom splash is large enough to overcome the surface tension. W_{cmax}/D is considered to be independent of V_i^2

because We_c for the head separation is constant in this case.

3.4 Splash formation of Type-III

A typical sequence of splash formation with $V_i = 4.9$ m/s, $Re = 1.1 \times 10^5$, and $We = 6.4 \times 10^3$ is shown in Fig. 9. The crown-type splash is observed at $T = 0.55$. The height of the crown increases, and a bulky air column forms behind the sphere at $T = 0.91$. The crown increases further in height, droplets fly in the radial direction, and longitudinal ridges on the surface of the air column is observed at $T = 1.82$. The formation of an air column between a solid sphere and non-Newtonian fluid was studied by Akers et al. (2006). They observed no ridges on the surface of the air column, which implies that the fluid properties affect the air column formation. As the crown starts to close, more droplets are generated, and ripples appear on the surface of the air column at $T = 3.03$. Truscott et al. (2006) investigated the air cavity in water formed by a spinning spherical body plunging into water. According to their results, the air column tilts because of spinning. As our spherical body is not spinning, the air column is straight and perpendicular to the water surface, as observed in Fig. 9. Figure 10 is the top view of the splash under the same condition as that in Fig. 9 at $T = 0.55$ and 0.91. The initial droplets fly radially and water jets that compose the crown grow at $T = 0.55$. The claw-like water jets grow together at $T = 0.91$. In this case, there are seven water jets, which are much less than the number of fingers predicted from the result shown in Fig. 7. Thus, we speculate that the water jets were formed by coalescing fingers. It is interesting that the number of the water jets is the same as the longitudinal ridges observed on the surface of air column. However, the reason why the water jets and ridges are formed is yet unclear.

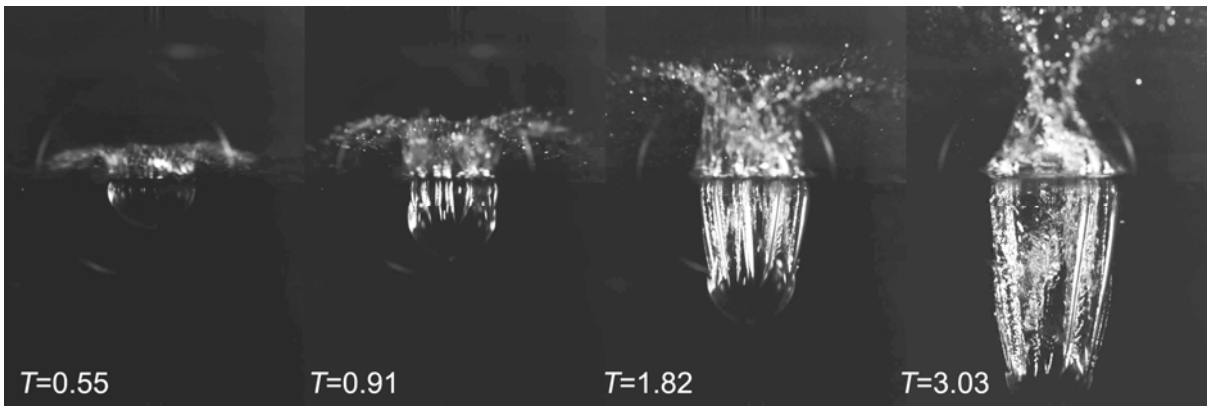

Fig.9 Sequence of Type-III splash formation at $V_i = 4.9$ m/s.

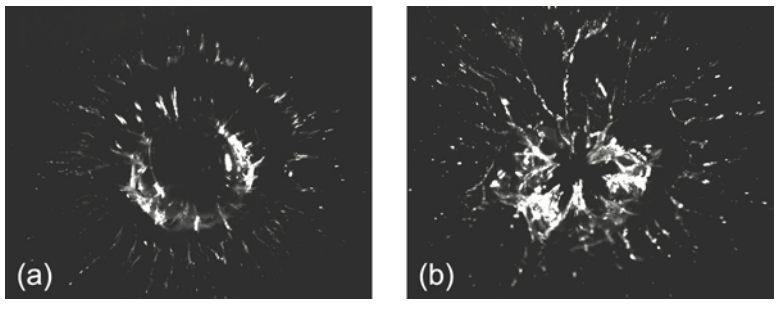

Fig.10 Top view of Type-III splashes due to impacts at $V_i = 4.9$ m/s. (a) $T = 0.55$ and (b) $T = 0.91$.

4. Conclusions

The splash caused by the impacting sphere on the water surface was investigated using a high speed

CMOS camera. We categorized the types of splash by impact velocities of the sphere. Three types of splash were found: Type-I is a thin spire-type splash, Type-II is a mushroom-type splash with many droplets, and Type-III is a crown-type splash with many droplets.

A Type-I thin spire-type splash was found to be generated when a concave water surface attached behind the sphere detached itself from the top of the sphere. The Type-II mushroom-type splash with many droplets was generated by a film flow climbing up the top of the sphere. Thus, the velocity of the film flow was found to be an important parameter for characterizing the splash and droplets. Droplets separated from the fingers at the top of the film flow and their separation was found to be related to the impact velocity of the sphere. Other droplets originated from a lower height of film flow, and the separation angle decreases for increasing impact velocity of the sphere for Type-II splashes. The number of droplets coincides with the number of fingers of film flow. The number of fingers can be predicted by Rayleigh–Taylor instability theory and increased with increasing impact velocity. The maximum height of the mushroom-type splash increased in proportion to the square of the impact velocity. This indicated that the kinetic energy of the impacting sphere transferred to the potential energy of the splash. The Type-III crown-type splash was characterized by water jets with many droplets. A bulky air column in the water was formed behind the sinking sphere. Longitudinal ridges and ripples were observed on the surface of the air column. It was found that the number of water jets coincide with that of the ridges.

References

Allen. R. F., The role of surface tension in splashing., Journal of Colloid and Interface Science, 51 (1975), 350-351.
Akers, B. and Belmote, A., Impact dynamics of a solid sphere falling into a viscoelastic micellar fluid, Journal of Non-Newtonian Fluid Mechanics, 135 (2006), 97-108.
Bejan, A. and Gobin, D., Constructal theory of droplet impact theory, International Journal of Heat and Mass Transfer, 49 (2006), 2412-2419.
Brussmann, M., Chandra, S., and Mostaghimi, J., Modeling the splash of a droplet impacting a solid surface, Physics of Fluids, 12 (2000), 3121-3132.
Duez, C. Y., Clanet, C. and Bocquet, L., Making a splash with water repellency, Nature Physics, 3 (2007), 180-183.
Kim, H. Y., Feng, Z. C. and Chun, J. H., Instability of a liquid jet emerging from a droplet upon collision with a solid surface, Physics of Fluids, 12(2000), 531-539.
Testik, F. Y., and Young, D. M., Breakup Patterns for Binary Drop Collisions, Journal of Visualization, 11-1 (2008), 4.
Truscott, T. T. and Techt, A. H., Cavity formation in the wake of spinning of sphere impacting the free surface, Physic of Fluids. 18 (2006), 091113-1.
von, Karman, The impact on seaplane floats during landing, National Advisory Committee for Aeronautics Technical Note, 321 (1929).
Worthington, A. M., On Impact with a Liquid Surface, Proceedings of the Royal Society of London, 34(1882-1883), 217-230
Yoon, S. S., Jepsen, R. A., Nissen, M. R. and O'Hern, T. J., Experimental investigation on splashing and nonlinear fingerlike instability of large water drops, Journal of Fluids and Structure, 23 (2007), 101-115.
Yoshida, T., Critical Breakup of a Liquid Droplet Due to Airstreams, Transactions of the Japan Society of Mechanical Engineers. B, 63(1997), 3580-3587.

Author Profile

Yoshihiro Kubota: He received his M.S. in Mechanical and Aerospace Engineering in 2008 from Syracuse University. He also received his M.Eng. degree in Department of Mechanical Engineering in 2005 from Graduate School of Toyo University. He joined in Biomechanical Engineering Laboratory, Toyo University in 2002. His research interests are Flow Visualization, PIV measurement.

Osamu Mochizuki: He worked in System Robotics, Toyo University as a professor from 2003 to 2008. He works in Department of Biomedical Engineering since 2009. His research interests are flow induced by small life, bio mimetics and PIV measurements.